J. Water Environ. Nanotechnol., 9(1): 73-89 Winter 2024

ORIGINAL RESEARCH PAPER

Comparative adsorption study of functionalized magnetite and maghemite nanoparticles coated with ctab surfactant for efficient chromium removal from wastewater

Mohamed Naous[1,2]*, Ahmed Halfadji[1,3]

[1] *Department of Sciences and Technology, Faculty of Applied Sciences, Ibn Khaldoun University of Tiaret, Tiare 14000, Algeria*
[2] *Laboratoire de Chimie Physique Macromoléculaire L.C.P.M, Université Oran, El-Menaouer, Oran, Algeria*
[3] *Synthesis and Catalysis Laboratory, Ibn Khaldoun University of Tiaret, Tiaret 14000, Algeria*

Received: 2023-08-03 Accepted: 2023-10-01 Published: 2024-01-31

ABSTRACT
In this study, maghemite and magnetite nanoparticles were functionalized with cetyl trimethyl ammonium bromide(CTAB) surfactants, to obtain effective chromium removal from wastewater. X-ray diffractometry (XRD), transmission electron microscopy (TEM), and Fourier-transform infrared spectrophotometry (FTIR) were used to characterize the functionalized nanoparticles. Various parameters, including pH, initial chromium concentration, added salt, and adsorbent dose, were evaluated in batch experiments to evaluate chromium removal efficiency. Adsorbent dose and chromium ions show a synergistic relationship with pH and the chemical and electrostatic interactions between cationic surfactant and negatively charged Cr(VI) ions. In both types of functionalized nanoparticles, Cr(VI) was efficiently removed at low pH values with CTAB@MNPs, but the pH increase negatively impacted the removal process. Additionally, Fe_3O_4@CTAB mainly adsorbs chromium chemically, reducing Cr(VI) to Cr(III), with less impact from competitive ions compared with γ-Fe_2O_3@CTAB.
At pH = 2, adsorbent dose = 5 g/L, and initial chromium concentration = 1 mg/L, maghemite@CTAB achieved a high chromium removal efficiency of 95%. In contrast, magnetite@CTAB achieved a chromium removal efficiency of 95.77% in 7 minutes and 30 seconds at pH = 4, adsorbent dose = 12 g/L, and initial chromium concentration = 98 mg/L. Notably, magnetite outperformed maghemite by a factor of 100 in chromium elimination, which can be attributed to the presence of two adsorption mechanisms, chemical, and physisorption, in magnetite nanoparticles, whereas maghemite only had physisorption.

Keywords: *Maghemite nanoparticles, Magnetite nanoparticles, Cetyl trimethyl ammonium bromide (CTAB) surfactants, Chromium removal, Adsorption efficiency, pH optimization*

How to cite this article
Naous M., Halfadji A., Comparative Adsorption Study of Functionalized Magnetite and Maghemite Nanoparticles Coated with CTAB Surfactant for Efficient Chromium Removal from Wastewater. J. Water Environ. Nanotechnol., 2024; 9(1): 73-89.
DOI: 10.22090/jwent.2024.01.05

INTRODUCTION

Chromium, particularly in its hexavalent form (Cr(VI)), is well-known for its high toxicity and carcinogenic properties, posing significant threats to both the environment and human health[1, 2]. Its presence in water sources can be attributed to natural occurrences, mainly resulting from the dissolution of minerals during the weathering of chromites and other chromium-bearing minerals in bedrock and soil[3, 4]. Conventional methods for chromium removal from wastewater are often expensive and inefficient, necessitating the exploration of alternative approaches[5-8].

In recent years, magnetic nanoparticles, such as magnetite (Fe_3O_4) and maghemite, have gained considerable attention as potential solutions for extracting chromium VI from wastewater[9-14]. These nanoparticles offer a high surface area-to-volume ratio, providing numerous active sites for

* Corresponding Authors Email: *elzahraadz@yahoo.fr*

efficient adsorption. Their magnetic properties enable easy separation from treated water using an external magnetic field, simplifying the recovery process[15].

The extraction process involves dispersing magnetic nanoparticles into contaminated wastewater to facilitate contact with chromium ions. Through adsorption, the nanoparticles effectively bind with chromium, removing it from the water[16-19]. Subsequently, applying an external magnetic field attracts the magnetic nanoparticles carrying the adsorbed chromium, facilitating their easy separation from the water. The utilization of magnetic nanoparticles presents several advantages, such as reusability, leading to reduced operational costs and minimized waste generation[20, 21]. Additionally, their small size allows for efficient mixing and enhanced contact with contaminants, thereby improving extraction efficiency [22, 23].

Functionalizing magnetite nanoparticles for heavy metal extraction offers several benefits for environmental remediation[24]. The reasons for employing functionalization include enhanced adsorption capacity, improved selectivity, stability, and dispersibility to maximize contact with heavy metal ions, pH and temperature control, minimization of interference from other substances or competing ions, and facilitation of separation and recovery. Reusability is another notable advantage of functionalized magnetite nanoparticles[25-27].

Among the surfactant-functionalized magnetite nanoparticles, those with cationic surfactants have demonstrated significant potential in the extraction of chromium VI from contaminated sources[28]. These engineered nanoparticles possess unique characteristics primarily due to their nanoscale size and magnetic core elements, including maghemite (γ-Fe_2O_3), magnetite (Fe_3O_4), and cobalt ferrite ($CoFe_2O_4$). Magnetite (Fe_3O_4) and maghemite (γ-Fe_2O_3), in particular, have been extensively explored and favored for their ability to act as an electron donor, because of their Fe^{2+} state[29].

The exceptional properties of surfactant-functionalized magnetite nanoparticles offer enhanced selectivity for Cr(VI), even in the presence of competing ions[30]. This selectivity is crucial when dealing with complex environments containing multiple contaminants. The environmentally friendly design of surfactant functional groups ensures the sustainability of the extraction process, making it an eco-friendly approach for Cr(VI) removal. These functional groups serve as effective protection for the naked magnetite nanoparticles, preventing agglomeration and ensuring their stability during the extraction process [31, 32].

Using functionalized magnetite nanoparticles as sorbents provides numerous advantages over other nanosorbents without magnetic features. They offer shorter extraction times, higher binding capacities, and lower detection limits compared to nano adsorbents like carbon nanotubes, graphene, clay, and chitosan nanocomposites[33]. Moreover, the ease of manipulation through an external magnetic field simplifies the separation process, eliminating the need for additional time-consuming steps like filtration or centrifugation[34].

The experimental approach involves functionalizing magnetic nanoparticles with the chosen surfactants and assessing their adsorption capacity at water/alkane interfaces

The purpose of this research work is to compare the efficacy of chromium VI removal from wastewater using two different types of functionalized nanoparticles: magnetite nanoparticles functionalized with the cationic surfactant CTAB and maghemite nanoparticles functionalized with the same surfactant. The research aims to investigate the capacity, ion selectivity, and key factors influencing the adsorption of Cr(VI) from wastewater using the cationic surfactant CTAB on both magnetite and maghemite.

EXPERIMENTAL AND METHODS

Materials

The cationic surfactant Cetyl Trimethyl Ammonium Bromide (CTAB), was acquired from Merck in Kenilworth, NJ, United States. The chemicals Ferrous Chloride Tetrahydrate (FeCl2·4H2O), Ferric Chloride Hexahydrate (FeCl3·6H2O), Ammonia (NH3), Hydrochloric Acid (HCl), and Perchloric Acid (HClO4) were also purchased from Merck, France. Additionally, Hydrochloric Acid (HCl, 37%), 1,5-diphenylcarbazide (DPC, ≥99%), and Acetone (≥99%) were obtained from Tianjin Fuchen Chemical Reagents Factory in Tianjin, China. For the synthesis and rinsing of the magnetic nanoparticles (Fe_3O_4), double-distilled water and deionized water were used.

Magnetite Synthesis

To prepare magnetite nanoparticles (Fe_3O_4), a 100 ml equimolar mixture of iron chloride III ($FeCl_3$, 6 H_2O) and iron chloride II ($FeCl_2$, 4 H_2O) solutions was prepared. The mixture was stirred, and then sodium hydroxide (NaOH, 10M) was added drop by drop until a black color appeared. The mixture was left under uniform agitation for 2 hours. Subsequently, the resulting product was washed three times with distilled water. The Fe3O4 was then recovered using a magnet and dried in a vacuum oven at 60°C. Finally, the MNPs were stored in a glass container until further use[35].

Maghemite Synthesis

To synthesize Maghemite nanoparticles (γ-Fe_2O_3), a solution of iron consisting of 2.0 g of FeCl2•4H_2O and 5 g of $FeCl_3$•6H_2O is diluted in 30 ml of water. The iron mixture is then stirred using a magnetic stirrer and heated to 80°C. Gradually, a 15% ammonium hydroxide solution is added drop by drop to the mixture over 20 minutes to ensure a homogeneous reaction. The resulting mixture is further stirred at 80°C for an additional 40 minutes. Afterward, the product is washed three times with water and ethanol. Finally, the γ-Fe_2O_3 are recovered using a magnet and dried in a vacuum oven at 60°C. The dried γ-Fe_2O_3 can be stored in a glass container for future use.

Magnetite@CTABSynthesis

The preparation of Fe_3O_4@CTAB composite in a one-step co-precipitation method involves the following procedure[36]:

To synthesize CTAB-functionalized magnetite through a one-step process, begin by combining 0.5 g of iron(III) chloride (FeCl3•6H2O), 0.4 g of iron(II) chloride (FeCl2•4H2O), and 0.4 g of cetyltrimethylammonium bromide (CTAB) in 100 ml of distilled water under agitation until full dissolution. Subsequently, introduce a 25% ammonium hydroxide solution drop by drop until the solution turns black. Maintain agitation for 2 hours to ensure optimal synthesis. The pH of the mixed solution was adjusted by adding ammonium hydroxide (NH_4OH) drop by drop. As the pH was adjusted (around pH 9-10), a black precipitate of Fe_3O_4@CTAB composite formed. After the co-precipitation process, the Fe_3O_4@CTAB was washed to remove any unreacted species and impurities. This was achieved using magnetic separation methods. Finally, the washed composite was dried using a vacuum oven until a dry powder was obtained.

Maghemite@CTAB Synthesis

For the one-step preparation of γ-Fe_2O_3@CTAB, the following procedure is followed: 5 g of iron (III) chloride ($FeCl_3$, 6H_2O), 4 g of iron (II) chloride ($FeCl_2$, 4H_2O), and 0.5 g of CnTAB are dissolved in 60 ml of distilled water under continuous stirring at 80°C until complete dissolution. Subsequently, 40 ml of a 15% ammonium hydroxide solution is added dropwise over a 20-minute interval until a dark brown color appears. The mixture is further stirred for 40 minutes while maintaining the temperature at 80°C. The resulting γ-Fe_2O_3@ CTABare then rinsed three times with water and ethanol, separated using a magnet, and dried in a vacuum oven at 50°C. The dried γ-Fe_2O_3@ CTABcan be stored in a glass container for future use.

Characterization

The MNPs@-CTAB composite powder was subjected to several characterization techniques to understand its properties and structure.

X-ray Diffraction (XRD): The XRD patterns of the MNPs@-CTAB composite powder were obtained using the Rigaku MiniFlex600. The average crystal size was determined using the Scherrer formula, which relates the crystal size (d) to the full width at half maximum (FWHM) of a diffraction peak measured at 2θ. The Scherrer formula is given by[37]:

$$d = K\lambda / \beta * \cos\theta \quad (1)$$

In Equation (1):

- "d" represents the crystal size.
- "K" is the Scherrer constant with a value of 0.9.
- "λ" denotes the X-ray wavelength of Cu Kα radiation, with a value of 1.5418 Å.
- "β" is the FWHM of a diffraction peak measured at 2θ.
- "θ" indicates the diffraction angle.

Fourier Transform Infrared (FTIR) Spectroscopy: The FTIR spectra of the MNPs@CTAB composite were recorded using the JASCO FT/IR-4100 spectrometer (Jasco, Tokyo, Japan) within the range of 4000.6 to 399.1 cm^{-1}. This technique provides information about the functional groups present in the composite material.

Transmission Electron Microscopy (TEM): The morphology of the MNPs was examined using a

transmission electron microscope (FEI Tecnai G2 20, 200 kV TEM) located in Oregon, USA. TEM allows for the visualization of the structure and size of the nanoparticles.

pH Measurement: The pH of the solution was measured using a Jenway 3510 digital pH/mV meter from the UK.

Water Preparation: Deionized water was prepared using the Millipore Elix S with an Automatic Sanitization Module (Merck Millipore, Madrid, Spain).

The specific surface area was determined using the multi-point Brunauer-Emmett-Teller (BET) method. The specific surface area was characterized using an automated surface area and pore size analyzer (Quadrasorb SI, Quantachrome) The sample underwent outgassing at 110°C for 4 hours.

Methods

Adsorption Process: In preparation for adsorption experiments, a series of standard solutions with varying concentrations of chromium (VI) were meticulously crafted. These solutions encompassed concentrations of 0.40, 0.50, 0.60, 0.70, and 0.80 mg/L, all derived from a chromium (VI) standard solution initially at a concentration of 100 mg/L[38]. Different doses of Fe_3O_4@CTAB and γ-Fe_2O_3@CTAB nanoparticles, 4 mg, 8 mg, and 12 mg, as well as unfunctionalized Fe_3O_4 and γ-Fe_2O_3 nanoparticles, 4 mg, 8 mg, and 12 mg, were used in adsorption studies. The pH level of the solution was determined by adding these nanoparticles to 30 ml distilled water. For one hour, the resulting mixtures were subjected to ultrasonic treatment. In the meantime, a 0.5 ml solution of K_2CrO_4 was added to this mixture and followed by further ultrasonic treatment. Utilizing sonication with functionalized magnetite nanoparticles facilitates the efficient solubilization of MNps@ CTAB throughout the solution. Consequently, this process yields a substantial surface-to-volume ratio, leading to an enhancement in adsorption efficiency on the resultant surface. Samples from 5 ml were collected in various intervals of five, 10, and fifteen minutes to be stored at 4 C for 24 hours. Four ml of 2N sulfuric acid, 0.20 ml of 1.5-diphenylcarbazide solution UPC 1.5, and 0.80 ml distilled water were added to each sample taken the previous day. The filtrates, which exhibited distinct colors, were then subjected to UV-Vis spectroscopy at a wavelength of 540 nm to detect the presence of Cr(VI) ions. A reduction in color intensity signified the successful removal of Cr(VI) ions from the solution. These adsorption experiments had the objective of assessing the efficacy of Fe_3O_4@CTAB, γ-Fe_2O_3@CTAB, Fe_3O_4, and γ-Fe_2O_3 nanoparticles in eliminating Cr(VI) from water under different pH conditions. The presence of Cr(VI) ions was ascertained through a colorimetric assay.

pH effect

To assess the adsorption capability of the MNps@CTAB composite in different settings, experiments were conducted at various pH levels, including acidic, neutral, and alkaline. The pH of the samples was adjusted by adding either 0.01 N NaOH or 0.01 N HCl. The concentrations of Cr(VI) in the samples were determined from a calibration curve.

The percentage of Cr(VI) removal was calculated using the equation:

$$Re(\%) = (C_0 - Ce) / C0 * 100$$

where C_0 represents the initial concentration of Cr(VI) in mg/l, and Ce represents the residual concentration of Cr(VI) in solution in mg/l.

Moreover, the researchers examined the correlation between the initial concentration of Cr(VI) and the adsorption capacity of the MNPs@CTAB composite. Flasks containing 25 mL of Cr(VI) solution were supplemented with 8 mg/mL of MNPs@CnTAB nanoparticles, and the adsorption capacity of the metal ions onto the composite was assessed using the equations mentioned earlier.

Interfering Ions Effect

The researchers chose potassium nitrate salt to investigate its effect on the adsorption of Cr(VI). They added 0.025 g of the salt to 25 ml of distilled water at pH 4 and then added 0.2 g of MNPs@ CTAB nanoparticles. After ultrasonication, 0.5 ml of K_2CrO_4 chromate solution was added at different time intervals. The samples were stored for 24 hours, and after that, the concentration of Cr(VI) was determined using spectroscopic analysis.

Extraction of Chromium Cr(VI) from Real Samples

To assess the effectiveness of the method for quantifying and extracting Cr(VI) in real samples, two different water samples were selected from Ain Djenane's water source of the city Tiaret (Algeria) and a natural wetland in Northwestern Algeria (Sebkha of DayatMorsli). The presence

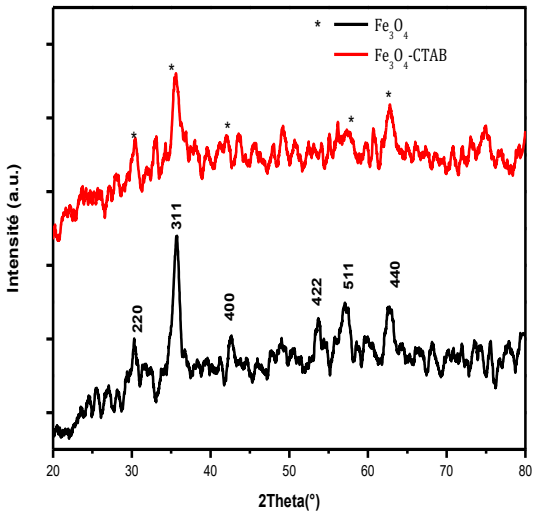

Fig. 1. X-ray diffraction patterns (XRD) of Fe3O4 nanoparticles and Fe3O4-CTAB.

Fig. 2. Formation of maghemite nanoparticles.

of Cr(VI) was confirmed in both samples using diphénylcarbazide 1,5 (DPC 1.5).

Additionally, air quality was analyzed by collecting air samples from an automobile traveling between Oran and Tiaret in Algeria. The samples were subjected to ultrasonic treatment and filtration, followed by the addition of MNPs nanoparticles. The sample's surface area is 5 cm^2 with a quantity of m = 0.53 g, and we place them in 25 ml of distilled water at pH = 4 for one hour in an ultrasonic bath. After filtration, we added a quantity of 12 mg/ml of previously used Fe_3O_4 into a sonicator for 1 hour. The concentration of Cr(VI) was determined using the same method mentioned earlier.

- We add 0.5 ml of K_2CrO_4 chromate solution.
- We take 5 ml at different time intervals (0; 1; 2.30; 5; 7.30 min).

These solutions are stored for 24 hours at 4°C. We add 4 ml of 2 N sulfuric acid plus 0.20 ml of 1.5 diphenylcarbazide solution (DPC 1.5) and 0.80 ml of distilled water into a 5 ml sample; we stir until the red-violet color appears (10 min).

RESULTS AND DISCUSSION

Structural/Microstructural Analysis

XRD (X-ray Diffraction)

The samples were analyzed with a powder X-ray diffractometer, and the XRD diagrams were measured from 20 to 80° (2θ) to reveal the nature of the sample.

Fig. 1 shows the XRD diagrams of Fe_3O_4 without CTAB (Cetyltrimethylammonium bromide) and Fe_3O_4 coated with CTAB. All XRD patterns were indexed for magnetite standards, confirming the formation of a cubic structure. The diffraction peaks at 30°, 35.4°, 43°, 53.4°, 56.9°, and 62.5° were associated with the (220), (311), (400), (422), (511), and (440) planes of the cubic unit cell, respectively. This analysis confirms that the synthesized particles have a magnetite crystal structure.

Moreover, the XRD pattern of Fe_3O_4@CTAB was found to be identical to that of Fe_3O_4, indicating that the phase structure of Fe_3O_4 remained unchanged after being coated with CTAB.

Additionally, the average crystal size of Fe_3O_4@CTAB was estimated using the Debye-Scherrer formula from the (311) peak, yielding a value of 11.61 nm. This result supports the functionalization of Fe_3O_4 with CTAB, contributing to an increase in the surface-to-volume ratio and the superparamagnetic nature of the nanoparticles (NPMs). These characteristics are significant for achieving a high percentage of Cr(VI) extraction, as discussed in the upcoming sections.

The maghemite obtained through co-precipitation can exhibit a color variation ranging from brown to dark brown, as depicted in Fig. 2. In Fig. 3, the typical XRD profile of γ-Fe2O3@CTABis presented, with the XRD data collected within the 2 theta range of 10 to 90 degrees. The analysis of the diffraction patterns revealed strong matches for various crystallographic planes, specifically 311, 422, 511, 220, 620, and 400. These planes showed excellent agreement with the maghemite phase, confirming the presence of this specific

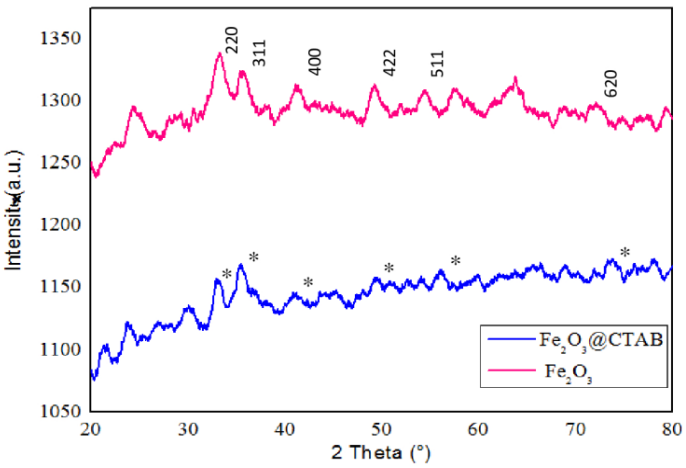

Fig. 3. XRD diffractogram of γ-Fe2O3 nanoparticles and γ-Fe2O3@CTAB

phase in the prepared γ-Fe2O3@CTABadsorbent. The XRD data indicated no evidence of any other phases, suggesting that the product formed is pure. Moreover, the observed diffraction peaks and their corresponding positions further support the crystalline nature of the synthesized material.

FTIR

The obtained Fe_3O_4@CTAB shows an absorption peak around 2837-3300 cm^{-1}, corresponding to the elongation vibration mode of OH groups adsorbed on the nanoparticle surface (Fig.4). This peak appears broad due to the formation of hydrogen bonding on the hydroxyl group. Additionally, there are peaks at 1462 and 1627 cm^{-1}, representing the in-plane and out-of-plane vibrations of O-H groups, respectively. The peak at 584 cm^{-1} corresponds to the Fe-O bond in Fe_3O_4.

In the 2800-3000 cm^{-1} region, the Fe_3O_4@CTAB exhibits vibrations corresponding to the elongation of CH bonds in alkyl groups. The asymmetric and symmetric vibrations of CH_2 groups are observed at 2914 and 2850 cm^{-1}, respectively. The asymmetric vibration of (CH3-N+) and C-N is observed at 3015 and 960 cm^{-1}, respectively. The peaks at 2848 and 2918 cm^{-1} are attributed to the vibrations of two different CH bands of CTAB. The peak at 2927.80 cm^{-1} indicates characteristic symmetrical and asymmetrical stretching vibrations of C-CH2 in the CTAB chain.

The obtained FTIR spectrum of the γ-Fe_2O_3@ CTAB nanoparticles displayed several distinct peaks indicative of their molecular interactions and vibrational characteristics. Here's a reformulation of the information provided:

The FTIR spectrum of the γ-Fe_2O_3@CTAB nanoparticles showed several peaks within specific regions. The peaks observed between 3300-3060 cm^{-1} were attributed to the electrostatic interaction between the hydroxyl groups of the ammonium fraction in CnTAB adsorbed on the surface of γ-Fe_2O_3 (OH^-...N+). Two other peaks were identified at 2915 and 2848 cm^{-1}, which were associated with the vibration of different CH bands of the -CH_2 group in CnTAB. Additionally, two peaks at 1607 and 1409 cm^{-1} corresponded to the asymmetric and symmetric stretching vibrations of N+CH_3, respectively. Another peak at 957 cm^{-1} was attributed to the out-of-plane CH vibration of CH3. Notably, a strong peak observed at 580 cm^{-1} indicated the presence of the Fe-O bond stretching vibration in γ-Fe_2O_3.

TEM

The Transmission Electron Microscope (TEM) image displayed in Fig. 5 reveals the presence of spherical-like particles with sizes ranging from 9 to 16 nm. By utilizing the Debye-Scherrer formula, researchers calculated the average crystallite size to be approximately 14 nm, which is consistent with the reported value. This finding presents essential insights into the size of the crystallites under investigation. The Debye-Scherrer formula, derived from X-ray diffraction analysis, allows for estimating the crystallite size based on the broadening of diffraction peaks. In this particular case, the calculated average crystallite size was determined to be around 13 nm.

Moreover, the study also demonstrates a strong agreement between the observed Fe_2O_3 particle

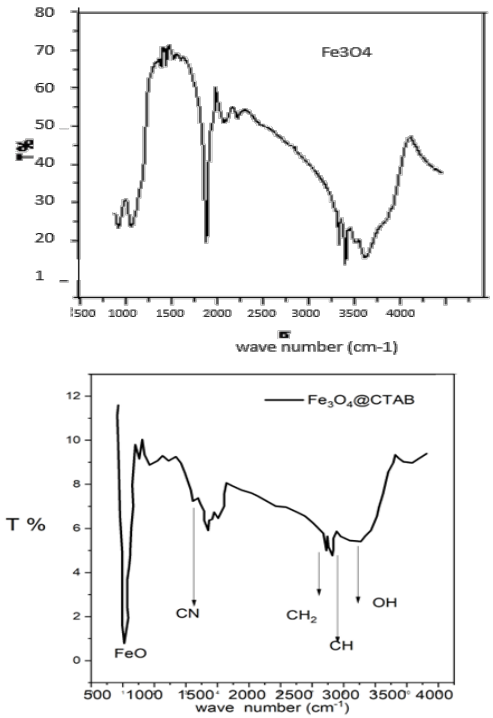

Fig. 4. FTIR Spectra of Fe_3O_4@CTAB and γ-Fe_2O_3@CTAB

Table 1: pH Effect on the adsorption of Cr(VI) at various concentrations of Fe3O4@CTAB nanoparticles after 7 minutes and 30 seconds of contact time.

PH	The quantity of Fe3O4@CTAB	RE %
PH = 4	4 mg/ml	87,07%
	8 mg/ml	90,06 %.
	12 mg/ml	95,77%
PH =9	4 mg/ml	84,01%
	8 mg/ml	83,60 %
	12 mg/ml	90,24%

sizes in the TEM image and those calculated from the XRD spectrum using the Scherrer formula.

Additionally, the provided information from another source shows that the Fe_3O_4/CTAB composite, which is magnetic nanoparticles capped with cetyltrimethylammonium bromide, exhibited high efficiency in removing Cr(VI) from contaminated water. The system achieved a maximum removal efficiency of 95.77% under acidic conditions (pH 4), with a contact time of 12 h and a composite dosage of 12 mg/mL :

The TEM image depicted in Fig. 5 revealed spherical-like particles with sizes ranging from 10 to 20 nm for the investigated α-Fe_2O_3 nanoparticles. The average crystallite size was calculated using the Debye-Scherrer formula and found to be approximately 14 nm. Interestingly, this result was consistent with a previously reported value.

The Debye-Scherrer formula, derived from X-ray diffraction analysis, is a valuable tool for estimating the size of crystallites based on the broadening of diffraction peaks. In this study, it was applied to determine the average crystallite size of the α-Fe_2O_3 nanoparticles, and the calculated value was around 14 nm. Remarkably, this size estimation was in strong agreement with the sizes of the Fe_2O_3 particles observed in the TEM image and those obtained from the XRD spectrum using the Scherrer formula.

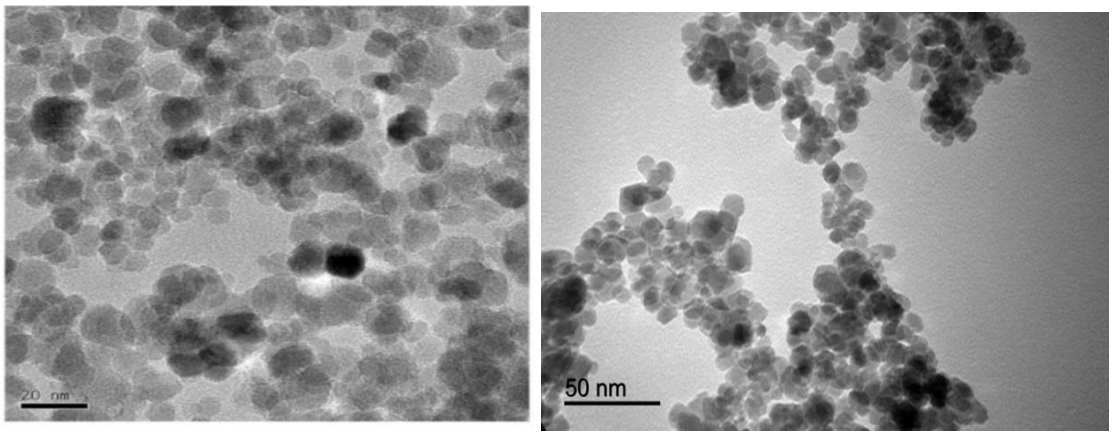

Fig. 5. TEM images of fMNPs@CTAB andγ-Fe_2O_3@CTAB

The agreement between the TEM image and the XRD analysis provides valuable information about the size of the crystallites in the investigated α-Fe_2O_3 nanoparticles, supporting the reliability of the characterization techniques employed in this research.

Effect of functionalization on adsorption

Notably, the elimination percentage of Cr(VI) using the Fe_3O_4@CTAB nanoparticles reached 97%, which was higher than the elimination achieved with other nanoparticles, as it did not exceed 87%.

The study demonstrates the potential of magnetic nanoparticles, such as Fe_3O_4, as efficient sorbents for the removal of various pollutants from aqueous solutions and effluents. The prepared nanoparticles were characterized through X-ray diffraction, transmission electron microscopy, Fourier transform infrared spectroscopy, and vibrating sample magnetometry, with diameters ranging from 10 to 15 nm. The adsorption of Ni(II) and Cr(VI) from diluted aqueous solutions onto Fe_3O_4 nanoparticles was investigated, and the removal efficiency was found to be highly dependent on solution pH.Cr(VI) removal was greater in the acidic range, while Ni(II) removal was more significant in the basic range of solutions.

The results obtained from the study reveal that the elimination percentage of chromium (VI) does not exceed 37%. This average efficiency may be attributed to the instability of non-functionalized maghemite nanoparticles, leading to a decrease in the surface-to-volume ratio and, consequently, a reduction in adsorption on their surfaces. However, when surfactant-functionalized nanoparticles, specifically γ-Fe_2O_3@CTAB, were used for the elimination of Cr(VI), they achieved an impressive removal efficiency of 97%. This significant enhancement in removal efficiency is highlighted in the subsequent section of the study.

The average specific surface area is 79.318±0.577 m^2/g for Fe_3O_4@CTAB and 80.213±0.687 m^2/g for γ-Fe_2O_3@CTAB. This value indicates that the sample did not aggregate due to CTAB functionalization. It's worth noting that both magnetite and maghemite nanoparticles retained their magnetic properties after vacuum drying treatment, leading to a relatively high specific surface area value.

Without ultrasonic radiation, we did not achieve a homogeneous mixture, and the adsorption yielded only 68% and 71% in chromium elimination percentage Fe_3O_4@CTAB and γ-Fe_2O_3@CTAB respectively under the following conditions: at pH = 4 for. After filtration, we added a quantity of 12 mg/ml of previously used Fe_3O_4@CTAB and γ-Fe_2O_3@CTAB (Fig. 6). The concentration of Cr(VI) was determined using the same method mentioned earlier.

The contrast between the elimination percentages observed for non-functionalized maghemite nanoparticles and surfactant-functionalized nanoparticles, γ-Fe_2O_3@CTAB, provides valuable insights into the importance of surface modifications in enhancing the adsorption capabilities of nanoparticles for Cr(VI) removal from the system.

The provided information suggests that for a pH of 4, a time interval of 0 to 7 minutes and 30 seconds, and a fixed quantity of Fe_3O_4@CnTAB (8 mg/ml), three curves exhibited the same increasing trend, reaching a maximum after only 2 minutes, as shown in Fig. 9. This observation indicates a strong

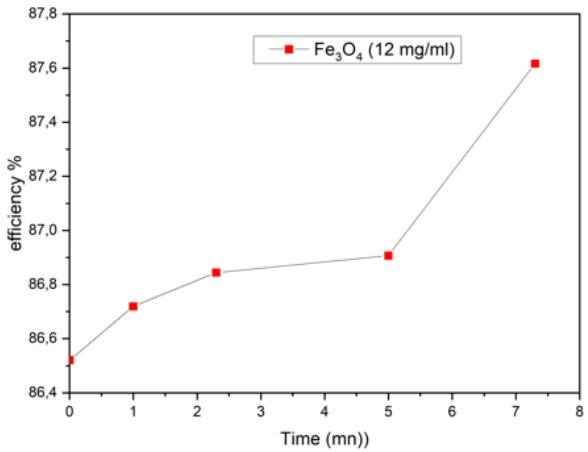

Fig. 6. The percentage of Cr(VI) elimination using a dose of 12 mg/mL of Fe3O4 nanoparticles at pH=4

interaction between Cr(VI) and the adsorbent Fe_3O_4@CnTAB. Three types of interactions were identified:

· Electrostatic Attraction:

This force arises between CrO_4H^- formed in the acidic environment (pH = 4) and the N+ of the ammonium group. The strength of this force increases with the length of the hydrophobic chain of the cationic surfactant attached to the Fe_3O_4 nanoparticle. Studies have shown that the diameter of NPMs@CnTAB varies inversely with the length of the hydrocarbon chain, leading to better Cr(VI) adsorption due to an increased surface-to-volume ratio. The hydrophobic effect also explains the variation in the percentage of Cr(VI) extraction with the chain length, as it causes the hydrophobic chain to move away from water molecules, reducing steric hindrance during the interaction of CrO4H- with the cationic head of the surfactant.

· *Chemisorption:*

This force exists between the iron core and Cr(VI), shedding light on the strong adsorption capability of the Fe_3O_4@CnTAB nanocomposite for Cr(VI) removal under acidic conditions. This makes it a promising candidate for effective water treatment in the presence of Cr(VI) contaminants.

pH effect

The study investigated the effect of different pH values (3 and 9) on the adsorption of Cr(VI) by nanoparticles (Fe_3O_4@CTAB) with a contact time of 7 minutes and 30 seconds (Table 1). Various doses of the adsorbent (4, 8, and 12 mg/ml) were used to remove Cr(VI) ions (98 mg/l) within the specified contact time. The results revealed that

the maximum adsorption of Cr(VI) occurred at pH=4 after 7 minutes and 30 seconds of contact time. It was observed that the Fe_3O_4@CTAB compound exhibited higher adsorption efficiency at an acidic medium (pH = 4) compared to a basic medium (pH = 9).

At pH 4, the eliminated amount of Cr(VI) using the adsorbent Fe_3O_4@CTAB (8 mg/ml) was 90.06%, whereas at pH 9, it was 83.60%. This difference in adsorption performance is attributed to the following factors:

1. Electrostatic Attraction: In an acidic environment (pH=4), the nanocomposite is positively charged due to the action of the protonated amine group (N+) of CTAB. This positive charge facilitates the adsorption of the negatively charged $HCrO_4^-$ ions through electrostatic attraction. However, at a basic pH (pH= 9), the excess OH- ions in the solution may compete with the metallic ions for binding sites on the Fe_3O_4@CTAB composite, leading to repulsion forces between the adsorbent surface and the Cr(VI) metal ion.

2. Reduction Reaction: In an acidic environment, electrons can be transferred from Fe^{2+} (located in the core of MNP Fe_3O_4) to Cr(VI), resulting in the reduction of Cr(VI) to insoluble Cr(III) hydroxide on the surface of magnetite. The reduction reaction is represented as follows: $Cr^{6+} + 3Fe^{2+} \Leftrightarrow Cr^{3+} + 3Fe^{3+}$. Additionally, free radical electrons can form due to the magnetic field generated by MNPs, which may enhance the chemical adsorption of $HCrO^{4-}$ anions in the solution by the iron cations at the core of the MNP.

Overall, the study highlights that Fe_3O_4@CTAB nanoparticles exhibit better Cr(VI) adsorption efficiency in an acidic environment (pH=4) due to the positive charge and reduction reactions,

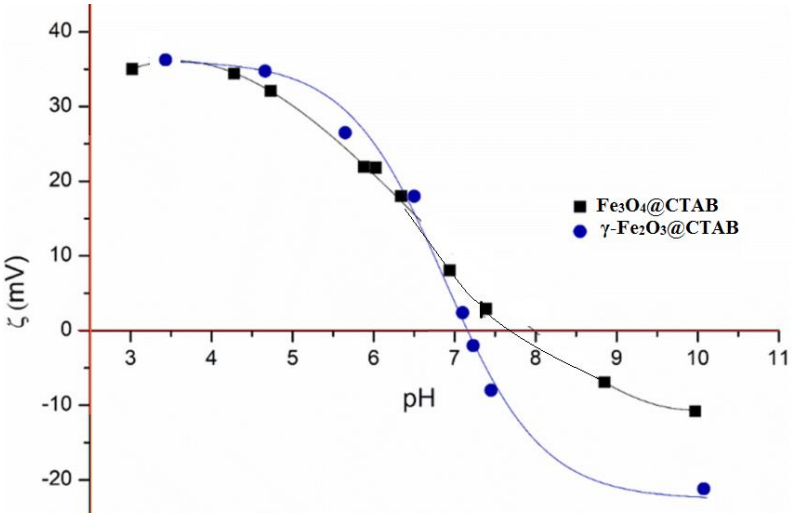

Fig. 7. Zeta potential of CTAB@Fe3O4 and CTAB@yFe$_2$0$_3$

while the adsorption efficiency decreases in a basic environment (pH=9) due to the presence of OH^- ions and repulsion forces.

The adsorption progression of Cr(VI) is influenced by the pH of the sample, which leads to protonation and deprotonation of the adsorbent surface functional groups.

on the other hand, and for the Fe3O4@CTAB. To investigate this effect, different pH values (2, 7, and 9) were studied during a 15-minute contact time with nanoparticles at concentrations of 4, 8, and 12 mg/mL. The results from Table 2 demonstrate that the maximum adsorption of Cr(VI) occurs at pH= 2 for the adsorbents during the 15-minute contact time.

According to Table 2, the composite γ-Fe_2O_3@ CTAB exhibits higher adsorption efficiency compared to γ-Fe_2O_3 at acidic pH 2. The highest removal efficiency was achieved at pH=2, with a maximum elimination of 95% of Cr(VI) after a 15-minute contact time.

Specifically, the γ-Fe_2O_3@CTAB composite exhibits higher adsorption efficiency in an acidic medium at pH=2. For the same quantity of adsorbent (4 mg/mL), the elimination of Cr(VI) reaches 84% and 78% in basic (pH=9) and neutral (pH=7) media, respectively. However, at pH=2, the elimination increases significantly, reaching up to 95%.

The preferential elimination of Cr(VI) in an acidic environment can be attributed to the positive charge acquired by the nanocomposite due to the protonated amine group (N+) of CTAB. The positively charged nanocomposite readily attracts and adsorbs the negatively charged $HCrO_4^-$ ions through electrostatic interactions. Conversely, in a basic environment, excess OH^- ions compete with metal ions for binding to the anion exchange sites of the γ-Fe_2O_3@CTAB composite, leading to repulsion between the adsorbent surface and the Cr(VI) ions. The presence of free radicals and the magnetic field generated by the magnetic nanoparticles (MNPs) contribute to the formation of electron radicals, supporting the results of Cr(VI) removal by the nanocomposites at alkaline pH=9. Additionally, electrostatic attraction between the surface-bound CTAB and Cr(VI) ions enhances the chemical adsorption of $HCrO_4^-$ anions by the iron cations at the core of the MNPs. The influence of high pH on metal removal is related to the formation of soluble metal complexes and their stability in aqueous solutions.

Electrostatic interactions can exert a significant influence on adsorption processes. Chromic acid exhibits two distinct pKa values, namely 0.74 and 6.50. Meanwhile, the isoelectric point (ZPC) of both γ-Fe_2O_3@CTAB and Fe_3O_4@CTAB falls within the pH range of 6 to 7. Below the ZPC pH, the particle surfaces acquire a positive charge, while Cr(VI) primarily exists in its dianionic form. In this context, the positively charged Fe_3O_4@CTAB and γ-Fe_2O_3@CTAB materials interact with negatively charged (CrO_4^{2-}) and mono-anionic (HCrO4-) forms within the pH range of approximately 2 to 6.5. Consequently, under mildly acidic conditions, attractive electrostatic interactions occur between

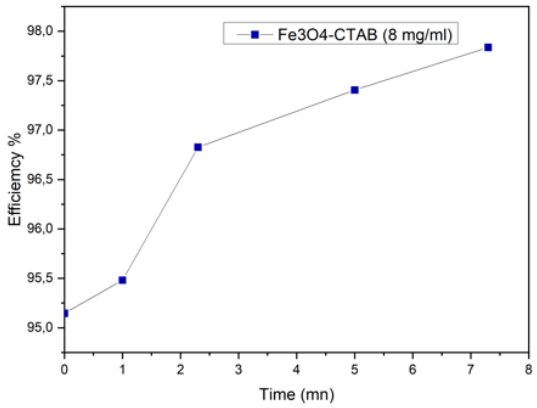

Fig. 8. The elimination percentage of Cr(VI) using a dose of 8 mg/mL of Fe_3O_4@CTAB nanoparticles at pH= 4 (KNO_3 salt).

Table 2: Adsorption of Cr at by γ-Fe_2O_3@CTAB different pH real samples

	PH=2	PH=7	PH=9
% of Cr (VI) removed	95%	78%	84%

Table 3 :Second order kinetics parameteres

	q_e(mg.g^{-1})	k_2 (g.mg^{-1}.h^{-1})	χ2	R^2
Fe_3O_4@CTAB	9.482	7.672	0.009	0.999
γ-Fe_2O_3@CTAB	9.472	11.383	0.012	0.999

the negatively charged Cr(VI) species and the positively charged surfaces, leading to favorable adsorption processes (Fig. 7). Above the pH of ZPC, the particle surface processes an overall negative charge while the dominant species of Cr(VI) is CrO_4^{2-} and thus under basic conditions electrostatic repulsion exists and poor adsorption is observed. While pH can have a pronounced influence on adsorption, effective removal can be achieved over a significant pH range from 2 to 9.

Salt effect

The presence of competitive ions, such as KNO_3 at a concentration of 1g/l, did not significantly affect the adsorption of Cr(VI) ions at a concentration of 98 ppm. The adsorption process exhibited high selectivity of Fe_3O_4@ CTAB for Cr(VI) ions, with a remarkable 98% elimination of Cr(VI) achieved in just 7 minutes and 30 seconds.

In other words, the Fe_3O_4@CTAB composite demonstrated efficient Cr(VI) removal even in the presence of competitive ions like KNO_3 as shown in Fig. 8. The adsorbent exhibited strong affinity and specificity for Cr(VI) ions, resulting in a high percentage of Cr(VI) elimination within a short contact time.

This finding highlights the potential of Fe_3O_4@ CTAB as a promising adsorbent for the effective and rapid removal of Cr(VI) from contaminated water, even in the presence of interfering ions, making it a valuable candidate for water treatment applications.

The presence of competitive ions, specifically potassium nitrate (KNO_3) at a concentration of 0.01 g/L, had a slight effect on the adsorption of Cr(VI) ions. The adsorption process exhibited a remarkable indication of the high selectivity of γ-Fe2O3@CTAB for Cr(VI) ions. After 15 minutes, the percentage of Cr(VI) removal reached 65% in the presence of KNO_3 ions, whereas it reached 95% in the absence of KNO_3 ions. The presence of salts, like KNO_3, influenced the adsorption of Cr(VI) ions, leading to a decrease in adsorption efficiency by 32%.

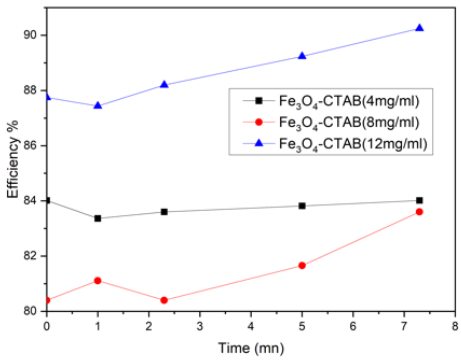

Fig. 9. Removal of Cr(VI) using varying quantities of Fe_3O_4@ CTAB.

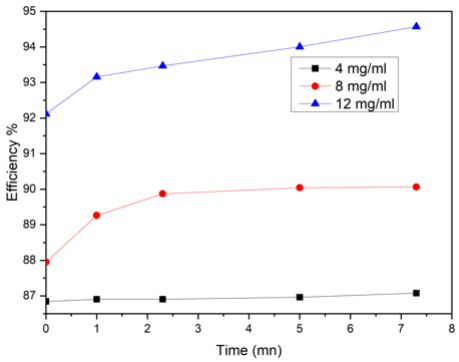

Fig. 10. Cr(VI) elimination as a function of contact time for various quantities of Fe_3O_4@CTAB (a) (4 mg/ml), (b) (8 mg/ml), and (c) (12 mg/ml) of Fe_3O_4/CTAB nanoparticles at pH = 4.

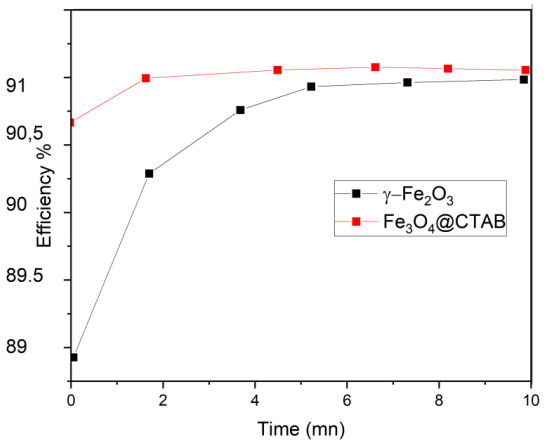

Fig. 11. Kinetic study at pH=3

Effect of the dosage of nanocomposites

It was observed that the removal of Cr(VI) ions increases proportionally with the concentration of Fe_3O_4@CTAB (Fig. 9). The optimal dosage of Fe_3O_4@CTAB was found to be 12 mg/ml, at which point an impressive 95.77% of Cr(VI) ions could be eliminated within a contact time of 7 minutes and 30 seconds at pH =9. This increase in the percentage of Cr(VI) removal (Fig. 10) can be attributed to the enhanced surface area available for interaction with the increasing amount of the adsorbent.

In summary, increasing the concentration of Fe_3O_4@CTAB resulted in higher efficiency in removing Cr(VI) ions. The optimal dose of 12 mg/ml at pH 9 allowed for the highest percentage of Cr(VI) elimination, showcasing the importance of the adsorbent dosage in the efficient removal of Cr(VI) from aqueous solutions.

Two adsorbents, with concentrations of 4, 8, and 12 mg/mL, were tested for the removal of Cr(VI) ions at room temperature (25.0°C ± 1.0°C) and various contact times.

The removal efficiency of Cr(VI) ions decreased as the concentration of both adsorbents increased. The optimal dosage of the γ-Fe_2O_3@CTAB composite (4 mg/mL) resulted in the elimination of 94% of Cr(VI) after 15 minutes of contact time. In contrast, the dosage of γ-Fe_2O_3 adsorbent (12 mg/mL) removed 84% of Cr(VI) under the same conditions. The intermediate dosage (8 mg/mL) of γ-Fe_2O_3@CTAB nanoparticles demonstrated a removal efficiency of 87% for Cr(VI).

Isotherm study

When conducting experiments at pH 3 and 25°C to investigate the impact of initial Cr(VI) concentration for both functionalized magnetic nanoparticles, it was observed that the equilibrium adsorption data aligns most closely with the Freundlich adsorption isotherm model. The

Table 4: Quantity of Cr (VI) found in real samples.

Studied samples	The air filter of the car	Domestic water of Ain El-djnan	Water of the Sebkha of Oran
Amount of Cr(VI) (in ppm)	13,72	2,15	2,03

Table. 5 presents a comparison of the removal capacity of Chromium VI by nanoparticulate adsorbents.

	maximum removal capacity [Cr(VI)]mg/g	Reference
[maghemite] = 0.3 g/L	5mg/g	Chromium(VI) removal by maghemite nanoparticles[40]
5 g/L of maghemite nanoparticles at pH 2.5	10	Removal and recovery of Cr(VI) from wastewater by maghemite nanoparticles [39]
Superparamagnetic nanoparticles/sludge biomass-derived activated carbon composite	80.21	A composite adsorbent of superparamagnetic nanoparticles with sludge biomass-derived activated carbon for the removal of chromium (VI) [41]
hydrogel-based magnetite nanocomposite	0.3	Synthesis and characterization of hydrogel-based magnetite nanocomposite adsorbents for the potential removal of Acid Orange 10 dye and Cr(VI) ions from aqueous solution[42]
biochar modified with magnetite nanoparticles	0.2	Effect of biochar modified with magnetite nanoparticles and HNO_3 for efficient removal of Cr(VI) from contaminated water: A batch and column scale study[43]
Maghemite@CTAB	12	Current work
magnetite@CTAB	125	Current work

Freundlich adsorption model is described by Equation 3.

$$q_e = K_F C_e^{\frac{1}{n}} \quad \text{Eq. 3}$$

In this equation, qe represents the amount of adsorbate adsorbed per unit mass of the adsorbent surface in milligrams per gram ($mg.g^{-1}$), while Ce represents the equilibrium concentration of the adsorbate in milligrams per liter ($mg.L^{-1}$). The model includes two constants, K_F and 1/n, which are associated with the adsorption capacity and adsorption intensity of the adsorbent, respectively. Equation 4 presents the linearized form of the

$$\log q_e = \log K_f + \frac{1}{n} \log C_e \quad \text{Eq. 4}$$

KF and 1/n are determined from the intercepts and slope of the Freundlich adsorption isotherm plot. For the removal of Cr(VI) from aqueous solutions at 298 K and pH 3, KF is found to be 24.76 (in units of $(mg/g)(L/mg)^{1/3}$), while the value of 1/n is 0.3985. These values suggest that the adsorption process is favorable, and the adsorption capacity increases as the number of adsorption sites increases.

Kinetic study:

Experiments were conducted to investigate the kinetics of Cr(VI) adsorption onto Fe_3O_4@CTAB and γ-Fe_2O_3@CTAB under conditions of pH 3 and an initial adsorbate concentration of 8 mg/ml. The rate of Cr(VI) removal by both functionalized magnetic nanoparticles was modeled using second-order rate equations. The determination of whether the obtained kinetics data aligns better with the second-order rate expression is achieved through the assessment of the regression coefficient of linear fit (R^2) and the non-linear fit Chi-square (χ^2). The χ2 value is a measure of the difference between the experimental adsorption capacity (qe(E)) and the theoretical adsorption capacity (qe(C)), as defined by equation 5.

$$\chi 2 = \sum \left(\frac{(q_e(E) - q_e(C))}{q_e(C)} \right) \quad \text{Eq. 5}$$

A smaller χ2 value corresponds to a better-fitted adsorption rate expression. Through this statistical analysis, we determined that the rate data fits very well with the pseudo-second-order rate equation 6.

$$\frac{1}{q_t} = \frac{1}{k_2 q_e^2} + \frac{1}{q_e} t \quad \text{Eq. 6}$$

In this equation, k_2 ($g.mg^{-1}.h^{-1}$) represents the rate constant, and $k_2 q_e^2$ ($mg.g^{-1}.h^{-1}$) is the initial adsorption rate. The fitted graph is presented in Fig.

11. Linear plots of t/q_t versus t confirmed that the adsorption process follows second-order kinetics. Table 3 provides the second adsorption kinetics parameters for the adsorption of Cr(VI) ions by Fe_3O_4@CTAB and γ-Fe_2O_3@CTAB.

In Fig. 11, an increase in adsorption capacity over time is depicted. Initially, the adsorption capacity exhibits rapid growth. However, after the initial adsorption stage, this capacity increases at a slower rate. This phenomenon can be elucidated as follows: In the initial stages, vacant or active adsorption sites are readily available to adsorb molecules. Consequently, during these early stages, the adsorption capacity shows rapid augmentation. However, over time, two factors come into play. First, there is the phenomenon of adsorbate-adsorbate repulsion, and second, there is a decrease in the availability of vacant adsorbent surface active sites. Consequently, after a certain duration, the adsorption capacity reaches a state of saturation or equilibrium.

The impact of contact time on the adsorption of Cr(VI) onto Fe_3O_4@CTAB and γ-Fe_2O_3@CTAB was investigated in a batch system, to eliminate approximately 98 mg of Cr(VI) by 8 mg/ml of adsorbent. Kinetics studies were conducted at a pH of 3, as this pH range exhibited the maximum adsorption capacity. The concentration of adsorbed Cr(VI) was plotted against time, as presented in Fig. 11. The adsorption curve displayed a rapid initial phase, where approximately 90% of Cr(VI) ions were removed within the first minute of contact time. Subsequently, the removal rate gradually slowed down, reaching equilibrium at t_eq = 10 minutes. Beyond this point, the concentration of adsorbed cations remained relatively stable over time. This rapid adsorption behavior can be attributed to the presence of active sites on the external surface of functionalized magnetic nanoparticles. These findings align with previous studies reported in the literature, such as Hu et al.[39], who observed an equilibrium time of 14 minutes for the adsorption of Cr(VI) ions onto maghemite nanoparticles. The amine functional group, located in the CTAB molecule, is identified as the primary adsorption site for anionic Cr(VI) aqueous species. The protonation-deprotonation equilibrium constant of these surface sites is determined through a modeling approach.

Real samples

To assess the effectiveness and specificity of our adsorption and analysis protocol for Cr (VI), we selected three real samples for testing:

· Ambient air: An air filter was used from a 2018 registered car (symbol 1.2) that had been in circulation for over a year, especially between the Algerian cities of Oran and Tiaret. Pieces of the filter were subjected to sonication for one hour before conducting UV analysis and testing the extraction protocol using Fe_3O_4@CTAB. We attempted to utilize the method presented in this study (Cr VI extraction by Magnetite@CTAB and its quantification through UV spectroscopy) to assess its effectiveness in extracting and quantifying chromium VI probably retained in the air filters of vehicles circulating within metropolitan areas, such as the city of Oran in Algeria. Oran is an industrial and, at the same time, touristically vibrant and densely populated city, increasing the risk of heavy metal pollution like chromium VI. Furthermore, the experimental method is straightforward, involving the procurement of a used car air filter from a vehicle circulating in this city during a specific period.

· Spring water from Ain El-Djnan, Tiaret, without any prior treatment.

· Sebkha water from Oran (DayatelMorsli) after filtration.

These samples were subjected to specific preparation procedures before analyzing the quantity of Cr (VI) present in each of them.

The results of this study indicate that Cr (VI) is indeed present in the local environment at a concerning level. The use of Fe_3O_4@CTAB for the elimination of Cr (VI) from water samples of Tiaret (Ain El-djnan), Oran sebkha, and the air filter showed rapid extraction efficiency. Over 95% of the added Cr (VI) was removed within just 7 minutes and 30 seconds, at a pH of 4, and with an adsorbent concentration of 8 mg/mL (Table. 4).

Comparative study

Table. 5 presents a comparison of the removal capacity of Chromium VI by nanoparticulate adsorbents.

CONCLUSION

The γ-Fe_2O_3 and Fe_3O_4 nanoparticles were successfully synthesized and functionalized with cationic surfactants, namely cetyltrimethylammonium bromide, through a one-step coprecipitation method. Sure! Here's the reformulated version of the provided information:

The experimental study confirmed the superparamagnetic nature of hybrid nanoparticles and evaluated their effectiveness in removing the toxic heavy metal, Cr(VI). The research established that maghemite and magnetite are efficient materials for Cr(VI) adsorption in water. Notably, magnetite demonstrated a 10 times greater elimination of chromium compared to maghemite, attributed to the coexistence of chemical and physisorption mechanisms in magnetite nanoparticles.

The adsorption performance depends on specific environmental conditions and material characteristics. Key findings from the optimization results are as follows:

- Effective extraction occurs in neutral and basic environments, with significant efficiency even in acidic conditions.
- An adsorbent dosage of 4 mg/mL is optimal for Cr(VI) concentrations ranging from 0 to 1 mg/L.
- The method remains effective even in the presence of salts.
- The extraction process is relatively rapid, requiring only a few minutes of contact time for maximum efficiency.
- More than 95% of Cr(VI) is removed from different media.
- The method achieves a detection limit for Cr(VI) in the range of a few ppm.
- The extraction and analysis procedure utilizes standard laboratory equipment and does not require hazardous organic solvents.

The research highlights the potential of maghemite nanoparticles functionalized with cationic surfactants as an environmentally friendly and efficient approach for Cr(VI) removal from water. The simplicity, speed, and compatibility with routine laboratory apparatus make this method promising for future water treatment applications. Further investigations can explore the scalability and long-term stability of the adsorbent for practical implementation in real-world scenarios.

Declaration of Competing Interest

The authors declare that they have no known competing financial interests or personal relationships that could have appeared to influence the work reported in this paper.

CONFLICT OF INTEREST

The authors hereby declare that there is no conflict of interest.

REFERENCES

[1] P. Sharma, S.P. Singh, S.K. Parakh, Y.W. Tong, Health hazards of hexavalent chromium (Cr (VI)) and its microbial reduction, Bioengineered, 13 (2022) 4923-4938. https://doi.org/10.1080/21655979.2022.2037273

[2] S. Ambika, M. Kumar, L. Pisharody, M. Malhotra, G. Kumar, V. Sreedharan, L. Singh, P. Nidheesh, A. Bhatnagar, Modified biochar as a green adsorbent for removal of hexavalent chromium from various environmental matrices: mechanisms, methods, and prospects, Chemical Engineering Journal, 439 (2022) 135716. https://doi.org/10.1016/j.cej.2022.135716

[3] C. Oze, S. Fendorf, D.K. Bird, R.G. Coleman, Chromium geochemistry of serpentine soils, International Geology Review, 46 (2004) 97-126. https://doi.org/10.2747/0020-6814.46.2.97

[4] D. Traoré, A. Beauvais, F. Chabaux, C. Peiffert, J.-C. Parisot, J.-P. Ambrosi, F. Colin, Chemical and physical transfers in an ultramafic rock weathering profile: Part 1. Supergene dissolution of Pt-bearing chromite, American Mineralogist, 93 (2008) 22-30. https://doi.org/10.2138/am.2008.2605

[5] A.S. Adeleye, J.R. Conway, K. Garner, Y. Huang, Y. Su, A.A. Keller, Engineered nanomaterials for water treatment and remediation: Costs, benefits, and applicability, Chemical Engineering Journal, 286 (2016) 640-662. https://doi.org/10.1016/j.cej.2015.10.105

[6] A. Saha, P. Mukherjee, K. Roy, K. Sen, T. Sanyal, A review on phyto-remediation by aquatic macrophytes: A natural promising tool for sustainable management of ecosystem, International Journal of Experimental Research and Review, 27 (2022) 9-31. https://doi.org/10.52756/ijerr.2022.v27.002

[7] M. Adams, A. Ghaly, Maximizing sustainability of the Costa Rican coffee industry, Journal of Cleaner Production, 15 (2007) 1716-1729. https://doi.org/10.1016/j.jclepro.2006.08.013

[8] R. Eizi, T.R. Bastami, V. Mahmoudi, A. Ayati, H. Babaei, Facile ultrasound-assisted synthesis of CuFe-Layered double hydroxides/g-C3N4 nanocomposite for alizarin red S sono-sorption, Journal of the Taiwan Institute of Chemical Engineers, 145 (2023) 104844. https://doi.org/10.1016/j.jtice.2023.104844

[9] A.M. Muliwa, T.Y. Leswifi, M.S. Onyango, A. Maity, Magnetic adsorption separation (MAS) process: An alternative method of extracting Cr (VI) from aqueous solution using polypyrrole coated Fe3O4 nanocomposites, Separation and Purification Technology, 158 (2016) 250-258. https://doi.org/10.1016/j.seppur.2015.12.021

[10] L. Joseph, B.-M. Jun, J.R. Flora, C.M. Park, Y. Yoon, Removal of heavy metals from water sources in the developing world using low-cost materials: A review, Chemosphere, 229 (2019) 142-159. https://doi.org/10.1016/j.chemosphere.2019.04.198

[11] A.O. Ezzat, M.S. Ali, H.A. Al-Lohedan, Synthesis, Characterization, and Application of Magnetite Nanoparticles Coated with Hydrophobic Polyethyleneimine for Oil Spill Cleaning, Journal of Chemistry, 2022 (2022). https://doi.org/10.1155/2022/3368298

[12] S. Bahrani, S.A. Hashemi, S.M. Mousavi, Environmental Applications of Magnetic Alloy Nanoparticles and Their Polymer Nanocomposites,

in: Handbook of Magnetic Hybrid Nanoalloys and their Nanocomposites, Springer, 2022, pp. 975-1006. https://doi.org/10.1007/978-3-030-90948-2_31

[13] A.Z.M. Badruddoza, Z.B.Z. Shawon, M.T. Rahman, K.W. Hao, K. Hidajat, M.S. Uddin, Ionically modified magnetic nanomaterials for arsenic and chromium removal from water, Chemical Engineering Journal, 225 (2013) 607-615. https://doi.org/10.1016/j.cej.2013.03.114

[14] T.R. Bastami, S. Khaknahad, M. Malekshahi, Sonochemical versus reverse-precipitation synthesis of Cu x O/Fe 2 O 3/MoC nano-hybrid: removal of reactive dyes and evaluation of smartphone for colorimetric detection of organic dyes in water media, Environmental Science and Pollution Research, 27 (2020) 9364-9381. https://doi.org/10.1007/s11356-019-07368-0

[15] M. Faraji, Recent analytical applications of magnetic nanoparticles, Nanochemistry Research, 1 (2016) 264-290.

[16] S. Chatterjee, S. Mahanty, P. Das, P. Chaudhuri, S. Das, Biofabrication of iron oxide nanoparticles using manglicolous fungus Aspergillus niger BSC-1 and removal of Cr (VI) from aqueous solution, Chemical Engineering Journal, 385 (2020) 123790. https://doi.org/10.1016/j.cej.2019.123790

[17] S.M. Pourmortazavi, H. Sahebi, H. Zandavar, S. Mirsadeghi, Fabrication of Fe3O4 nanoparticles coated by extracted shrimp peels chitosan as sustainable adsorbents for removal of chromium contaminates from wastewater: The design of experiment, Composites Part B: Engineering, 175 (2019) 107130. https://doi.org/10.1016/j.compositesb.2019.107130

[18] S. Lal, A. Singhal, P. Kumari, Exploring carbonaceous nanomaterials for arsenic and chromium removal from wastewater, Journal of Water Process Engineering, 36 (2020) 101276. https://doi.org/10.1016/j.jwpe.2020.101276

[19] T. Wang, S. Ai, Y. Zhou, Z. Luo, C. Dai, Y. Yang, J. Zhang, H. Huang, S. Luo, L. Luo, Adsorption of agricultural wastewater contaminated with antibiotics, pesticides and toxic metals by functionalized magnetic nanoparticles, Journal of Environmental Chemical Engineering, 6 (2018) 6468-6478. https://doi.org/10.1016/j.jece.2018.10.014

[20] P. Somu, U. Kannan, S. Paul, Biomolecule functionalized magnetite nanoparticles efficiently adsorb and remove heavy metals from contaminated water, Journal of Chemical Technology & Biotechnology, 94 (2019) 2009-2022. https://doi.org/10.1002/jctb.5984

[21] K. Gupta, P. Joshi, R. Gusain, O.P. Khatri, Recent advances in adsorptive removal of heavy metal and metalloid ions by metal oxide-based nanomaterials, Coordination Chemistry Reviews, 445 (2021) 214100. https://doi.org/10.1016/j.ccr.2021.214100

[22] J. Garvasis, A.R. Prasad, K. Shamsheera, T.N. Roy, A. Joseph, A facile one-pot synthesis of phyto-conjugate superparamagnetic magnetite nanoparticles for the rapid removal of hexavalent chromium from water bodies, Materials Research Bulletin, 160 (2023) 112130. https://doi.org/10.1016/j.materresbull.2022.112130

[23] M. Najafi, T.R. Bastami, N. Binesh, A. Ayati, S. Emamverdi, Sono-sorption versus adsorption for the removal of congo red from aqueous solution using NiFeLDH/Au nanocomposite: Kinetics, thermodynamics, isotherm studies, and optimization of process parameters, Journal of Industrial and Engineering Chemistry, 116 (2022) 489-503. https://doi.org/10.1016/j.jiec.2022.09.039

[24] R.K. Gautam, S. Soni, M.C. Chattopadhyaya, Functionalized magnetic nanoparticles for environmental remediation, in: Handbook of research on diverse applications of nanotechnology in biomedicine, chemistry, and engineering, IGI Global, 2015, pp. 518-551. https://doi.org/10.4018/978-1-4666-6363-3.ch024

[25] A.M. Abu-Dief, S.M. Abdel-Fatah, Development and functionalization of magnetic nanoparticles as powerful and green catalysts for organic synthesis, Beni-Suef University Journal of Basic and Applied Sciences, 7 (2018) 55-67. https://doi.org/10.1016/j.bjbas.2017.05.008

[26] V. Singh, K. Rakshit, S. Rathee, S. Angmo, S. Kaushal, P. Garg, J.H. Chung, R. Sandhir, R.S. Sangwan, N. Singhal, Metallic/bimetallic magnetic nanoparticle functionalization for immobilization of α-amylase for enhanced reusability in bio-catalytic processes, Bioresource technology, 214 (2016) 528-533. https://doi.org/10.1016/j.biortech.2016.05.002

[27] A. Soozanipour, A. Taheri-Kafrani, M. Barkhori, M. Nasrollahzadeh, Preparation of a stable and robust nanobiocatalyst by efficiently immobilizing of pectinase onto cyanuric chloride-functionalized chitosan grafted magnetic nanoparticles, Journal of colloid and interface science, 536 (2019) 261-270. https://doi.org/10.1016/j.jcis.2018.10.053

[28] S. Chaudhary, P. Sharma, D. Singh, A. Umar, R. Kumar, Chemical and pathogenic cleanup of wastewater using surface-functionalized CeO2 nanoparticles, ACS Sustainable Chemistry & Engineering, 5 (2017) 6803-6816. https://doi.org/10.1021/acssuschemeng.7b01041

[29] K. Ahmouda, Green synthesis and characterization of iron oxide nanoparticles: evaluation of the reactivity of their surfaces, in, Universty of Eloued, 2022.

[30] S.A. Elfeky, S.E. Mahmoud, A.F. Youssef, Applications of CTAB modified magnetic nanoparticles for removal of chromium (VI) from contaminated water, Journal of advanced research, 8 (2017) 435-443. https://doi.org/10.1016/j.jare.2017.06.002

[31] J. You, L. Wang, Y. Zhao, W. Bao, A review of amino-functionalized magnetic nanoparticles for water treatment: Features and prospects, Journal of Cleaner Production, 281 (2021) 124668. https://doi.org/10.1016/j.jclepro.2020.124668

[32] M.S. Samuel, E. Selvarajan, R. Chidambaram, H. Patel, K. Brindhadevi, Clean approach for chromium removal in aqueous environments and role of nanomaterials in bioremediation: Present research and future perspective, Chemosphere, 284 (2021) 131368. https://doi.org/10.1016/j.chemosphere.2021.131368

[33] R. Saxena, M. Saxena, A. Lochab, Recent progress in nanomaterialsforadsorptiveremovaloforganiccontaminants from wastewater, ChemistrySelect, 5 (2020) 335-353. https://doi.org/10.1002/slct.201903542

[34] M. Sajid, Magnetic ionic liquids in analytical sample preparation: A literature review, TrAC Trends in Analytical Chemistry, 113 (2019) 210-223. https://doi.org/10.1016/j.trac.2019.02.007

[35] S.H. Araghi, M.H. Entezari, Amino-functionalized silica magnetite nanoparticles for the simultaneous removal of pollutants from aqueous solution, Applied Surface Science, 333 (2015) 68-77. https://doi.org/10.1016/j.apsusc.2015.01.211

[36] N. Li, H.-F. Zhang, J. Chen, Y.-P. Shi, One-step in situ preparation of Fe3O4/carboxylated multi-walled carbon nanotube hybrid for the determination of caffeine in carbonated beverages, Bulletin of the Chemical Society of Japan, 92 (2019) 290-296. https://doi.org/10.1246/bcsj.20180094

[37] A.W. Burton, K. Ong, T. Rea, I.Y. Chan, On the estimation of average crystallite size of zeolites from the Scherrer equation: A critical evaluation of its application to zeolites with one-dimensional pore systems, Microporous and Mesoporous Materials, 117 (2009) 75-90. https://doi.org/10.1016/j.micromeso.2008.06.010

[38] X. Lu, J. Duan, Y. Huang, Adsorption of Cr (VI) in Water with Phosphoric Acid Modified and Ordinary Walnut Shells, Agricultural Science & Technology, 16 (2015) 1989.

[39] J. Hu, G. Chen, I.M. Lo, Removal and recovery of Cr (VI) from wastewater by maghemite nanoparticles, Water Research, 39 (2005) 4528-4536. https://doi.org/10.1016/j.watres.2005.05.051

[40] W. Jiang, M. Pelaez, D.D. Dionysiou, M.H. Entezari, D. Tsoutsou, K. O'Shea, Chromium (VI) removal by maghemite nanoparticles, Chemical Engineering Journal, 222 (2013) 527-533. https://doi.org/10.1016/j.cej.2013.02.049

[41] A.M. Elgamal, N.A. Abd El-Ghany, G.R. Saad, Synthesis and characterization of hydrogel-based magnetite nanocomposite adsorbents for the potential removal of Acid Orange 10 dye and Cr (VI) ions from aqueous solution, International Journal of Biological Macromolecules, 227 (2023) 27-44. https://doi.org/10.1016/j.ijbiomac.2022.12.110

[42] V. Ramya, D. Murugan, C. Lajapathirai, S. Meenatchisundaram, S. Arumugam, A composite adsorbent of superparamagnetic nanoparticles with sludge biomass derived activated carbon for the removal of chromium (VI), Journal of Cleaner Production, 366 (2022) 132853. https://doi.org/10.1016/j.jclepro.2022.132853

[43] M. Imran, Z.U.H. Khan, M.M. Iqbal, J. Iqbal, N.S. Shah, S. Munawar, S. Ali, B. Murtaza, M.A. Naeem, M. Rizwan, Effect of biochar modified with magnetite nanoparticles and HNO3 for efficient removal of Cr (VI) from contaminated water: a batch and column scale study, Environmental Pollution, 261 (2020) 114231. https://doi.org/10.1016/j.envpol.2020.114231